NASA/TM–2017–219795

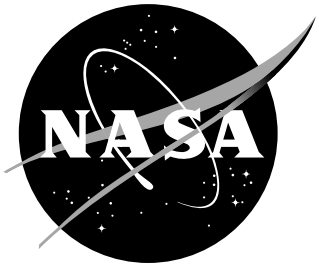

Position Corrections for Airspeed and Flow Angle Measurements on Fixed-Wing Aircraft

Jared A. Grauer
Langley Research Center, Hampton, Virginia

November 2017

The NASA STI Program Office ... in Profile

Since its founding, NASA has been dedicated to the advancement of aeronautics and space science. The NASA Scientific and Technical Information (STI) Program Office plays a key part in helping NASA maintain this important role.

The NASA STI Program Office is operated by Langley Research Center, the lead center for NASA's scientific and technical information. The NASA STI Program Office provides access to the NASA STI Database, the largest collection of aeronautical and space science STI in the world. The Program Office is also NASA's institutional mechanism for disseminating the results of its research and development activities. These results are published by NASA in the NASA STI Report Series, which includes the following report types:

- TECHNICAL PUBLICATION. Reports of completed research or a major significant phase of research that present the results of NASA programs and include extensive data or theoretical analysis. Includes compilations of significant scientific and technical data and information deemed to be of continuing reference value. NASA counterpart of peer-reviewed formal professional papers, but having less stringent limitations on manuscript length and extent of graphic presentations.
- TECHNICAL MEMORANDUM. Scientific and technical findings that are preliminary or of specialized interest, e.g., quick release reports, working papers, and bibliographies that contain minimal annotation. Does not contain extensive analysis.
- CONTRACTOR REPORT. Scientific and technical findings by NASA-sponsored contractors and grantees.
- CONFERENCE PUBLICATION. Collected papers from scientific and technical conferences, symposia, seminars, or other meetings sponsored or co-sponsored by NASA.
- SPECIAL PUBLICATION. Scientific, technical, or historical information from NASA programs, projects, and missions, often concerned with subjects having substantial public interest.
- TECHNICAL TRANSLATION. English-language translations of foreign scientific and technical material pertinent to NASA's mission.

Specialized services that complement the STI Program Office's diverse offerings include creating custom thesauri, building customized databases, organizing and publishing research results ... even providing videos.

For more information about the NASA STI Program Office, see the following:

- Access the NASA STI Program Home Page at ***http://www.sti.nasa.gov***
- E-mail your question via the Internet to help@sti.nasa.gov
- Fax your question to the NASA STI Help Desk at (301) 621–0134
- Phone the NASA STI Help Desk at (301) 621–0390
- Write to:
  NASA STI Help Desk
  NASA Center for AeroSpace Information
  7115 Standard Drive
  Hanover, MD 21076–1320

NASA/TM–2017–219795

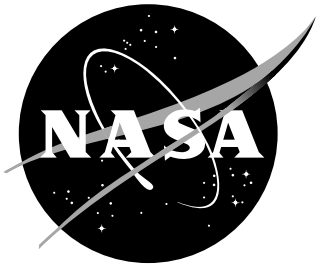

Position Corrections for Airspeed and Flow Angle Measurements on Fixed-Wing Aircraft

Jared A. Grauer
Langley Research Center, Hampton, Virginia

National Aeronautics and
Space Administration

Langley Research Center
Hampton, Virginia 23681-2199

November 2017

Available from:

NASA STI Program / Mail Stop 148
NASA Langley Research Center
Hampton, VA 23681-2199
Fax: 757-864-6500

Abstract

This report addresses position corrections made to airspeed and aerodynamic flow angle measurements on fixed-wing aircraft. These corrections remove the effects of angular rates, which contribute to the measurements when the sensors are installed away from the aircraft center of mass. Simplified corrections, which are routinely used in practice and assume small flow angles and angular rates, are reviewed. The exact, nonlinear corrections are then derived. The simplified corrections are sufficient in most situations; however, accuracy diminishes for smaller aircraft that incur higher angular rates, and for flight at high air flow angles. This is demonstrated using both flight test data and a nonlinear flight dynamics simulation of a subscale transport aircraft in a variety of low-speed, subsonic flight conditions.

Contents

Nomenclature

Roman

a, b, c	quadratic equation coefficients
b	wingspan, ft
$\bar{c}$	mean aerodynamic chord, ft
h	altitude, ft
$I_{..}$	inertia components, slug·ft^2
m	mass, slug
n	aircraft scale
p, q, r	body-axis rotational velocities, rad/s
S	wing reference area, ft^2
u, v, w	body-axis translational velocities, ft/s
V	true airspeed, ft/s
x, y, z	body-axis sensor positions, ft

Greek

α	angle of attack, rad
β	sideslip angle, rad
μ	flank angle, rad

Subscripts

0	trim value
a	angle of attack sensor
cm	center of mass
f	flank angle sensor
l	left wingtip
n	nose
p	pitot tube sensor
r	right wingtip
s	arbitrary sensor

1 Introduction

Aircraft used in research flight testing are typically instrumented with one or more airdata probes to provide information on true airspeed, angle of attack, sideslip angle, and other aerodynamic quantities. These probes are mounted on booms extending forward from the aircraft to measure the freestream airflow rather than the disturbed flow immediately surrounding the aircraft. The measured airspeed and flow angles parameterize the motion of the aircraft center of mass, but also contain contributions due to the rotational motion of the aircraft due to position offset of the sensors from the aircraft center of mass. Because many analyses require air-relative velocity information at the aircraft center of mass, corrections are applied to remove the angular rate contributions from the measured data. Many other corrections are also applied (e.g., to account for upwash, transport lags, boom bending, etc. [1–4]), but this report will focus only on the airdata sensor position corrections.

The position corrections commonly applied to flight test data involve several simplifying assumptions, such as small angles and low angular rates. Upon searching the technical literature, the author did not find any reports presenting the geometrically "exact" corrections for position offset without these simplifying assumptions. Rather, most sources advise that these simplified corrections are "adequate for most situations" [5]. One report [3] provided corrections that were not limited to small air flow angles, but made other approximations with regard to the angular rates.

To fill a perceived gap in the literature, this report contributes a derivation of the exact airdata sensor position corrections, without the application of small angle and low angular rate assumptions. Application of the exact and simplified position corrections to various aircraft and flight test data largely confirmed the conventional guidance that the simplifying assumptions are valid and accurate in the majority of cases. However, there were instances found using a subscale airplane in which significant differences resulted from applying the two sets of position corrections. These discrepancies were due to the development of relatively large angular rates, to which smaller aircraft are more prone, which violated the simplifying assumptions. Therefore, a more careful analysis of the airdata sensor position corrections is warranted when flying subscale models or agile aircraft, performing aerobatic maneuvers, or when analyzing flight records involving gusts, accidents, or loss-of-control events.

The remainder of this report is organized as follows. Section 2 reviews relevant nomenclature and definitions. Section 3 presents the simplified position corrections and the assumptions used. In Section 4, the exact position corrections are derived. Simulation and flight test examples of interest are presented in Section 5, and concluding remarks are discussed in Section 6.

2 Geometrical Relationships

The velocity experienced at an arbitrary point s on a rigid aircraft traveling in a non-moving atmosphere is

$$\begin{bmatrix} u_s \\ v_s \\ w_s \end{bmatrix} = \begin{bmatrix} u \\ v \\ w \end{bmatrix} + \begin{bmatrix} 0 & -r & q \\ r & 0 & -p \\ -q & p & 0 \end{bmatrix} \begin{bmatrix} x_s \\ y_s \\ z_s \end{bmatrix} \tag{1}$$

The terms u, v, and w are the body-axis components of translational velocity at the aircraft center of mass. The corresponding rotational velocity components are p, q, and r.

The position of the point relative to the aircraft center of mass is expressed in body axes components as x_s, y_s, and z_s.

Components of the velocity are measured using onboard sensors, placed at various points on the aircraft. For instance, pitot-static tubes mounted on airdata booms measure dynamic and static pressures. The true airspeed of the aircraft in low-speed flight can be computed from this information and knowledge of the ambient atmosphere. Ideally, airspeed measurements reflect the speed of the aircraft

$$V_p = \sqrt{u_p^2 + v_p^2 + w_p^2} \tag{2a}$$

where the subscript p indicates the measurement is taken at the pitot tube inlet location. It is assumed that the static pressure port is collocated with the pitot tube inlet so that the airspeed can be accurately computed from this information, and that measurements are not affected by high air flow angles or angular rates. Substituting expressions for the local velocities from Eq. (1) in Eq. (2a), the airspeed measurement becomes

$$V_p = \sqrt{\left(u - ry_p + qz_p\right)^2 + \left(v + rx_p - pz_p\right)^2 + \left(w - qx_p + py_p\right)^2} \tag{2b}$$

Another set of sensors, usually in the form of flow vanes, are mounted on airdata booms and become aligned with the local air flow to measure angle of attack and flank angle. Ignoring any measurement distortions, the angle of attack measurement can be defined and expanded in a similar manner as

$$\alpha_a = \arctan\left(\frac{w_a}{u_a}\right) \tag{3a}$$

$$= \arctan\left(\frac{w - qx_a + py_a}{u - ry_a + qz_a}\right) \tag{3b}$$

where the subscript a indicates the measurement is taken at the angle of attack vane. Likewise, the flank angle measurement is

$$\mu_f = \arctan\left(\frac{v_f}{u_f}\right) \tag{4a}$$

$$= \arctan\left(\frac{v + rx_f - pz_f}{u - ry_f + qz_f}\right) \tag{4b}$$

where the subscript f indicates the measurement is taken at the flank angle vane. The sideslip angle is related to the flank angle and angle of attack as

$$\beta = \arctan\left(\tan\mu\cos\alpha\right) \tag{5}$$

The sideslip angle, as opposed to the flank angle, is typically used in aerodynamic modeling. However, the flank angle is usually measured because it is mechanically simpler to do so, and because the two angles are approximately equal at low angles of attack. Note that there is not a standard nomenclature in the literature for the flank angle. This report uses μ, but other works may reuse the α or β characters with an additional subscript. Note also that in general these three measurements are not collocated but are instead made at different locations.

Expressing the airspeed and flow angle measurements in terms of u, v, w and p, q, r; as in Eqs. (2b), (3b), and (4b); explicitly shows the effect of the angular rates on the airspeed and flow angle measurements. The goal of the next section is to remove these angular rate components from the measurements and produce V, α, and β (or equivalently u, v, and w) at the aircraft center of mass, as is often used in flight dynamics and controls analyses.

3 Simplified Position Corrections

This section presents the simplified position corrections typically used to remove the contributions of angular rates from the measured data. These position corrections are reported in many works, for example in Refs. [1], [5], and [6]. The objective is to compute V, α, and β at the center of mass from recorded sensor data.

In contrast to the air flow angle data, the airspeed measurements are not typically corrected for the angular rate contributions. The value at the center of mass is therefore taken as the measurement

$$\boxed{V \simeq V_p} \tag{6}$$

One reason for this assumption is that for conventional airplanes, u is usually the dominant term in Eq. (2b), and is much larger than the angular rate contributions.

By a similar argument, the forward speed at the angle of attack vane is assumed to be much larger than the angular rate contributions, so that Eq. (1) simplifies to $u_a \simeq u$. Using this simplification and assuming small angles in the arctangent function, the angle of attack correction simplifies from Eq. (3b) to

$$\alpha_a \simeq \frac{w - qx_a + py_a}{u} \tag{7a}$$

$$= \frac{w}{u} + \frac{-qx_a + py_a}{u} \tag{7b}$$

$$\simeq \alpha + \frac{-qx_a + py_a}{u} \tag{7c}$$

Furthermore, for small flow angles $u \simeq V$ and the correction to the angle of attack measurement becomes

$$\boxed{\alpha = \alpha_a + \frac{qx_a - py_a}{V}} \tag{7d}$$

This last approximation uses the measured true airspeed from Eq. (6), rather than the aircraft forward speed, in the denominator of the correction equation and considerably reduces complexity.

A similar procedure is used to correct the flank angle measurements. Applying the same types of assumptions used for the angle of attack correction, the flank angle correction can be reduced as

$$\mu_f \simeq \frac{v + rx_f - pz_f}{V} \tag{8a}$$

$$= \frac{v}{V} + \frac{rx_f - pz_f}{V} \tag{8b}$$

$$\simeq \beta + \frac{rx_f - pz_f}{V} \tag{8c}$$

from which the corrected sideslip angle is

$$\boxed{\beta = \mu_f + \frac{pz_f - rx_f}{V}} \tag{8d}$$

Together, Eqs. (6), (7d), and (8d) represent the simplified equations used to correct airdata measurements to the aircraft center of mass. These equations only account for position corrections, and assume the aircraft experiences only small air flow angles and small angular rates. As noted in Ref. [5], these assumptions are appropriate for most situations. However, there are some cases in which these assumptions are not valid.

One such case is when air flow angles become large and small-angle approximations lose validity. Relative error of small-angle approximations for several trigonometric functions are shown in Fig. 1. The points marked in red indicate the angles at which 5% relative error is surpassed, which for most functions is above 20 deg. It can therefore be expected that when aircraft are flown in unusually high airflow angles, the simplified corrections should not be used on airspeed and air flow angle measurements. Some examples of this include aerobatic flight, loss-of-control scenarios, and in post-stall research maneuvers.

A second case is when the angular rate contributions become significant. As reported in Ref. [7] and illustrated in Fig. 2, as the size of an aircraft n decreases, the translational velocities decrease proportional to $n^{1/2}$ while the angular rates increase as $n^{-1/2}$. In other words, a smaller aircraft flies slower but rotates faster than a larger aircraft. When this happens, the assumption of small angular rates loses validity and the simplified position corrections degrade in accuracy.

An alternative method for correcting airspeed and flow angle data for position errors is to assume that these data are collocated. All three components of velocity would then be known at a single point, rather than at different points as in this report. Local values of V_s, α_s, and β_s can be converted to local values of u_s, v_s, and w_s (see Appendices A and B). These values are corrected to the center of mass as u, v, and w, then converted back to V, α, and β. These transformations are much simpler than the exact corrections discussed in the next section, but can lose accuracy as the aircraft scale increases and the sensors are located farther apart.

4 Exact Position Corrections

In this section, the exact position corrections for airspeed and flow angle measurements are derived. These relationships were determined by solving the three measurement equations (2b), (3b), and (4b) for the three unknowns u, v, and w. This was done algebraically using the method of substitution, wherein the equations were written in terms of one unknown and then were back-substituted to solve for the remaining unknowns. Afterwards, the corrected airspeed and flow angles were readily computed from the determined values of u, v, and w.

To begin, Eqs. (3b) and (4b) were rearranged to solve for w and v, respectively, in terms of u and the other variables as

$$v = (u - ry_f + qz_f)\tan\mu_f - rx_f + pz_f \tag{9}$$

$$w = (u - ry_a + qz_a)\tan\alpha_a + qx_a - py_a \tag{10}$$

These equations were then substituted into the (squared, for convenience) airspeed measurement Eq. (2b),

$$\begin{aligned} V_p^2 = {} & [u - ry_p + qz_p]^2 \\ & + [(u - ry_f + qz_f)\tan\mu_f + r(x_p - x_f) + p(z_f - z_p)]^2 \\ & + [(u - ry_a + qz_a)\tan\alpha_a + q(x_a - x_p) + p(y_p - y_a)]^2 \end{aligned} \tag{11}$$

Expanding this equation and grouping like terms yielded a quadratic equation in u of the form

$$au^2 + bu + c = 0 \tag{12a}$$

where the coefficients were defined

$$a = 1 + \tan^2\alpha_a + \tan^2\mu_f \tag{12b}$$

$$\begin{aligned} b = {} & 2qz_p - 2ry_p \\ & + 2(qz_a - ry_a)\tan^2\alpha_a + 2[p(y_p - y_a) + q(x_a - x_p)]\tan\alpha_a \\ & + 2(qz_f - ry_f)\tan^2\mu_f + 2[p(z_f - z_p) + r(x_p - x_f)]\tan\mu_f \end{aligned} \tag{12c}$$

$$\begin{aligned} c = {} & -V_p^2 \\ & + p^2\left[(y_p - y_a)^2 + (z_f - z_p)^2\right] \\ & + q^2\left[z_p^2 + z_a^2\tan^2\alpha_a + z_f^2\tan^2\mu_f + (x_a - x_p)^2 + 2z_a(x_a - x_p)\tan\alpha_a\right] \\ & + r^2\left[y_p^2 + y_a^2\tan^2\alpha_a + y_f^2\tan^2\mu_f + (x_p - x_f)^2 - 2y_f(x_p - x_f)\tan\mu_f\right] \\ & + 2pq\left[(x_a - x_p)(y_p - y_a) + z_a(y_p - y_a)\tan\alpha_a + z_f(z_f - z_p)\tan\mu_f\right] \\ & + 2pr\left[(x_p - x_f)(z_f - z_p) - y_a(y_p - y_a)\tan\alpha_a - y_f(z_f - z_p)\tan\mu_f\right] \\ & + 2qr\left[-y_pz_p - y_a(x_a - x_p)\tan\alpha_a - y_az_a\tan^2\alpha_a + z_f(x_p - x_f)\tan\mu_f - y_fz_f\tan^2\mu_f\right] \end{aligned} \tag{12d}$$

Examining this quadratic equation shows that many of the terms are due to the angular rates. As the angular rates decrease, $b \to 0$ and $c \to -V_p^2$, which recovers the standard transformation equations between V, α, μ and u, v, w provided in Appendix A. In addition, much of the complexity in the quadratic equation is reduced in the limit as sensors are placed closer to the center of mass (e.g., as $y_p \to 0$) and closer together (e.g., as $x_a \to x_p$).

When the aircraft is moving forward, as is the usual case with airplanes, the root of the quadratic equation

$$u = \frac{-b + \sqrt{b^2 - 4ac}}{2a} \tag{13}$$

is selected. For convenience, this closed-form solution is evaluated numerically at this point in the analysis, rather than continuing to expand its cumbersome analytical representation. After the value of u is computed, it is back-substituted into Eqs. (9) and (10) to obtain corresponding values of v and w.

With the translational velocities of the center of mass now known, the corrected airspeed and flow angles at the center of mass are

$$\boxed{\begin{aligned} V &= \sqrt{u^2 + v^2 + w^2} && \text{(14a)} \\ \alpha &= \arctan\left(\frac{w}{u}\right) && \text{(14b)} \\ \beta &= \arcsin\left(\frac{v}{V}\right) && \text{(14c)} \end{aligned}}$$

as provided in Appendix B.

Equations (14), together with Eqs. (9), (10), and (13), represent the exact position corrections for the airspeed and air flow angle measurements on a rigid aircraft. No assumptions of small angles or small angular rates were needed in this derivation. These exact corrections are considerably more complex than the simplified corrections, but accurately reflect the complicated relationships between the measured and desired quantities.

5 Flight Test and Simulation Examples

Test Aircraft and Nonlinear Simulation

The examples presented next use recorded flight test data from the NASA T-2 subscale airplane and simulated data from its nonlinear flight dynamics simulation. These sources of data were selected because the validity of the simplified airdata corrections degrades for subscale aircraft and for some of the maneuver types flown on this particular aircraft. Additionally, the flight test data included a wide variety of research maneuvers using research-grade instrumentation.

The T-2, pictured in Fig. 3, is a 5.5% dynamically-scaled model of a generic transport aircraft. It has twin jet engines mounted under the wings and retractable landing gear. The airplane was equipped with a micro inertial navigation system, which provided three-axis translational accelerometer measurements, angular rate measurements, estimated attitude angles, and Global Positioning System (GPS) velocity and position. A second inertial measurement unit gave additional accelerometer and gyroscope measurements with lower latency. Air flow angle vanes and pressure ports attached to booms mounted on each wingtip measured the angle of attack, flank angle, static pressure, and dynamic pressure. Measurements from static pressure sensors and ambient temperature sensors were used to compute air density and altitude. Engine speed was measured and used as input to an engine model to compute thrust. The engine model was identified from ground test data with adjustments for ram drag identified from flight data. Potentiometers on the rotation axes of the control surfaces were used to measure control surface deflections. Mass properties were computed based on measured fuel flow, preflight weight and balance, and inertia measurements done on the ground for the aircraft without fuel. The T-2 aircraft has 16 separate control surfaces. For the flight data analyzed in this work, only the conventional elevator, aileron, and rudder control surfaces were deflected. Physical parameters for the aircraft are given in Table 1.

The accompanying nonlinear flight dynamics simulation is called the Generic Transport Model Aircraft Nonlinear MATLAB Simulation based on Polynomial Aerodynamic and Engine Models (GTM POLYSIM) [8]. This simulation is based on the T-2 aircraft, and includes polynomial aerodynamic models obtained from wind tunnel test data using a similarly-shaped test article [9]. The wind tunnel data is valid for angles of attack from -5 to $+85$ deg; sideslip angles of ± 45 deg; nondimensional angular rate components of ± 0.107, ± 0.008, and ± 0.112 in roll, pitch, and yaw, respectively; elevator deflections from -30 to $+20$ deg; aileron deflections of ± 20 deg; and rudder deflections of ± 30 deg. In addition to the airdata sensors on each wing tip, a third set of airdata sensors (not existent on the T-2 airplane) was added to the airplane simulation at 2.5 fuselage diameters ahead of the nose.

In each example, orthogonal phase-optimized multisine inputs were applied simultaneously to the elevator, aileron, and rudder control surfaces. These computerized inputs were added to other inputs from the pilot and flight control system, just before actuator rate and position limiters. The inputs were designed to elicit uncorrelated and small-perturbation responses useful for dynamic modeling. More information about the optimized multisine inputs can be found, for example, in Ref. [6].

Nominal Maneuvers

The first example maneuver includes small perturbation excitations about trimmed flight at a low angle of attack. This is first shown using the GTM POLYSIM, with simulated data of the airspeed, angle of attack, flank/sideslip angle, and angular rates given in Fig. 4. In this plot and other sets that follow, the measured values are shown in green, whereas the simplified corrections are shown in blue and the exact corrections to these data are shown in red. An accompanying plot is also given, which shows the differences between the data corrected using the simplified corrections and the data corrected using the exact corrections.

For this case, the simplified corrections were accurate for the airspeed measurement on the nose-boom, all angle of attack measurements, and for all sideslip or flank angle measurements. However, the exact corrections removed significant content from the wing-tip airspeed data. For the airdata probes on the wings, x_p and z_p were approximately zero, and therefore $V_p^2 \simeq (u - ry)^2$. The effects of the yaw rate can be seen in the wing-tip airspeed time histories using the simplified correction. At the times where the yaw rate was positive, the airspeed value from the left wing was too high and the right wing was too low. The converse was true when the yaw rate was negative. Note also that when the exact corrections were applied, all corrected time histories for each quantity were similar in size and shape, despite the different location on the aircraft in which the measurement was taken.

Similar characteristics were seen in flight test data with the T-2 airplane, as shown in Fig. 5. Recall there is no nose-boom probe installed on the T-2, only sensors protruding from the wingtips. A significant effect of yaw rate was again evident in the airspeed measurements, and corrected sideslip angles were indistinguishable from each other. There were some differences between the simplified and exact corrections to the angle of attack time histories, and also between the left and right sensor data. However, these differences could be attributable to factors other than position errors, such as differing amounts of friction in the vanes or by spanwise fluctuations in the air flow.

The differences resulting from applying the simplified and exact corrections shown in this example were relatively small but could be important, depending on the application, for similar and smaller sized aircraft. For example, inaccuracies in the airspeed measurement increase uncertainty in the trim airspeed and the nondimensionalization of the angular rates for estimation of stability and control derivatives. Furthermore, the frequency of the phugoid mode is much closer to the short period mode for subscale aircraft than for full-sized aircraft, making the airspeed accuracy more important. If both wing tips were instrumented with airdata sensors and both were functioning well, measurements could be averaged to mitigate some of the error. This was done during flight testing of the T-2 and other aircraft, for example as in Ref. [10].

Effects of Gyroscope and Sensor Position Errors

Reference [5] recommends that "If you cannot convincingly demonstrate that a given correction will improve the data, then do not make the correction." In that spirit, the GTM POLYSIM was used to investigate the extent to which noise and uncertainty in the measured data degrades the simplified and exact position corrections.

In measured flight test data, gyroscope measurements of the angular rates are subject to measurement noise and bias errors. Similarly, relative locations of the sensor positions, computed from models of the center of mass based on fuel flow measurements and a schematic of

the aircraft, are also subject to uncertainty. Airspeed and flow angle measurements include a variety of errors as well, but these were not considered in this report.

Using the GTM POLYSIM, the nominal maneuver was again simulated but where gyroscope measurements were corrupted with a 1.0 deg/s random bias and white noise having standard deviation 1.0 deg/s. Sensor position measurement time histories were corrupted by a 0.25 inch random bias, resulting from uncertainty in center of mass positions computed from fuel flow and position measurements. Because sensor position information comes in part from integrating fuel-flow sensor data, measurement noise was neglected on these measurements. These errors are large compared to what is usually seen in typical flight test data and were used here to represent a worst-case scenario. One resulting simulation run is shown in Fig. 9. The time histories using the exact position corrections appeared noisier than those using the simplified corrections because they make more use of noisy and uncertain data. However, the exact corrections were also more accurate because the significant contributions of the angular rates were removed.

One approach to further reduce the error of the exact corrections is to smooth the measurements and remove the noise before applying the corrections [6]. Additionally, a data compatibility analysis could be applied to remove the biases from the gyroscope measurements [6]. These errors are usually small, however, and can often be safely ignored. Errors in the sensor positions generally cannot be improved without more accurate measurements or models, but are usually small as well.

Maneuvers at High Air Flow Angles with High Angular Rates

Three examples of T-2 flight test data at high air flow angles are given. In Figs. 7 and 8, small perturbation maneuvers are shown for trimmed flight at high angles of sideslip and at high angles of attack beyond stall, respectively. Feedback control was used in these cases to help the pilot maintain high nominal air flow angles. In Fig. 9, a slow approach to stall from trimmed level flight was performed while multisine excitations were applied.

For the high-sideslip maneuver, there was in general good agreement between the data processed using the simplified and the exact corrections. However, differences between the corrected sideslip angle time histories were larger than shown before in Fig. 5 because of the higher air flow angles. There were also larger differences in the peaks for the angle of attack data. The exact corrections adjusted the peaks of these data, whereas the simplified corrections were more similar to the measured data.

For the maneuver at high angles of attack, there were significant differences in the corrected angle of attack time histories, particularly between 15–20 s. During this time, large angular rates developed as a result of the aircraft flying under feedback control in the post-stall flight regime. These larger angular rates, as well as the larger air flow angles, diminished the accuracy of the simplified corrections. This was also true, to a lesser extent, of the sideslip data. Corrections to the airspeed data are not as evident in Fig. 8 as in previous plots because the variation in airspeed was much larger than for the previous maneuvers. The slow response in measured airspeed at 10 s, when the angle of attack abruptly increased to 25 deg, indicated that the pitot tubes installed on the aircraft were of good quality and did not have significant sensitivities to air flow angles within this range.

For the slow-stall maneuver, large differences between the corrected data were evident between 15–25 s, when the aircraft stalled and recovered. It was during this time that the aircraft experienced both large angular rates and large flow angles.

Each of these three cases showed an example where the data processed using the simplified corrections differed from those processed using the exact corrections. The primary factor for this was larger angular rates, although larger flow angles were also responsible to a lesser extent.

6 Concluding Remarks

This report examined the position corrections used to remove angular rate effects from airspeed and air flow angle measurements. The simplified correction equations typically used in practice were presented, which assume small angles and small angular rates. The exact correction equations, free of these assumptions, were then derived. Examples using a subscale aircraft and its nonlinear flight dynamics simulation were shown to illustrate cases where the simplified correction equations lose accuracy.

The primary contribution of this paper is the derivation and presentation of the exact position corrections for airspeed and aerodynamic flow angle measurements. These exact corrections were not found in the current literature, and remove additional contributions from the angular rates due to offset from the center of mass. Additional findings and suggestions were:

1. For subscale aircraft that incur relatively high angular rates, the exact position corrections should be applied to the airspeed and angle of attack data.
2. For the subscale aircraft simulation used, the exact position corrections were more accurate than the simplified position corrections when the data contained relatively large amounts of measurement noise and bias error.
3. With regard to position corrections only, sensors on the nose-boom had lower errors than sensors mounted on the wing tips.

7 Acknowledgements

This research was supported by the NASA Advanced Air Transport Technology project. Discussions with Dr. Eugene Morelli and Joaquim Neto Dias are acknowledged and appreciated. Mr. John Foster, Dr. Eugene Morelli, and Dr. John Ryan performed technical reviews of this report.

References

1. Gainer, T.; and Hoffman, S.: Summary of Transformation Equations and Equations of Motion Used in Free-Flight and Wind-Tunnel Data Reduction and Analysis. SP-3070, NASA, Hampton, VA, 1972.

2. Gracey, W.: Measurement of Aircraft Speed and Altitude. RP-1046, NASA, Hampton, VA, May 1980.

3. Haering, Jr., E.: Airdata Calibration of a High-Performance Aircraft for Measuring Atmospheric Wind Profiles. TM-101714, NASA, Edwards, CA, January 1990.

4. Haering, Jr., E.: Airdata Measurement and Calibration. TM-104316, NASA, Edwards, CA, December 1995.

5. Maine, R.; and Iliff, K.: Application of Parameter Estimation to Aircraft Stability and Control: The Output-Error Approach. RP-1168, NASA, Edwards, CA, June 1986.

6. Morelli, E.; and Klein, V.: *Aircraft System Identification: Theory and Practice*. Sunflyte Enterprises, Williamsburg, VA, second ed., 2016.

7. Wolowicz, C.; Bowman, Jr., J.; and Gilbert, W.: Similitude Requirements and Scaling Relationships as Applied to Model Testing. TP-1435, NASA, Edwards, CA, August 1979.

8. Morelli, E.: GTM POLYSIM — Nonlinear GTM Aircraft Polynomial Simulation in MATLAB, Version 2.0. NASA Software Catalog, 2007. Number LAR-17595-1.

9. Murch, A.: Generic Transport Model (GTM) Aircraft Nonlinear MATLAB Simulation based on Polynomial Aerodynamic and Engine Models (GTM POLYSIM). Simulation readme file, October 2007.

10. Moes, T.; and Whitmore, S.: A Preliminary Look at Techniques Used to Obtain Airdata From Flight at High Angles of Attack. TM-101729, NASA, Edwards, CA, December 1990.

A – Transforming V, α, μ to u, v, w

Given measurements of V, α, and μ at a single point, the corresponding values of u, v, and w can be found at that same point using the method of substitution. To solve this problem, the angle of attack and flank angle measurements were rearranged in terms of u and other variables as

$$v = u \tan \mu \tag{15}$$

$$w = u \tan \alpha \tag{16}$$

Substituting these equations into the (squared, for convenience) airspeed measurement resulted in

$$V^2 = u^2 + \left(u \tan^2 \mu\right)^2 + \left(u \tan^2 \alpha\right)^2 \tag{17}$$

Solving this quadratic equation for u, and then substituting the result back into the equations for v and w above yielded

$$u = \frac{V}{\sqrt{1 + \tan^2 \alpha + \tan^2 \mu}} \tag{18a}$$

$$v = \frac{V \tan \mu}{\sqrt{1 + \tan^2 \alpha + \tan^2 \mu}} \tag{18b}$$

$$w = \frac{V \tan \alpha}{\sqrt{1 + \tan^2 \alpha + \tan^2 \mu}} \tag{18c}$$

These equations are also given in Ref. [4].

This case was less complex than in Section 4 because the angular rates were not involved. This led to the quadratic form coefficients a and c in Eq. (12a) being much simpler, and $b = 0$. If it can be assumed that the airspeed and vane measurements are collocated, this method could be used to find u, v, and w at the sensor location (as shown earlier), and then use Eq. (1) to transform these values to the aircraft center of mass, from which V, α, and β can be computed.

B – Transforming V, α, β to u, v, w

The same procedure employed in Section 4 and Appendix A can be used to compute u, v, and w when given V, α, and β. In this case, the angle of attack and flank angle measurements were rearranged in terms of u and other variables as

$$v = \frac{u \sin\beta}{\cos\alpha \cos\beta} \tag{19}$$

$$w = u \tan\alpha \tag{20}$$

Substituting these equations into the (squared, for convenience) airspeed measurement resulted in

$$V^2 = u^2 + \left(\frac{u \sin\beta}{\cos\alpha \cos\beta}\right)^2 + \left(u \tan^2\alpha\right)^2 \tag{21}$$

which then yielded

$$u = V \cos\alpha \cos\beta \tag{22a}$$

$$v = V \sin\beta \tag{22b}$$

$$w = V \sin\alpha \cos\beta \tag{22c}$$

These are the conventional equations found in most texts on flight dynamics, for example Ref. [6].

Tables

Table 1: T-2 and GTM geometry and nominal mass properties

Group	Parameter	Value	Unit
Geometry	b	6.85	ft
	$\bar{c}$	0.92	ft
	S	5.90	ft^2
Mass[1]	m	1.64	slug
	I_{xx}	1.18	slug-ft^2
	I_{yy}	4.65	slug-ft^2
	I_{zz}	5.58	slug-ft^2
	I_{xz}	0.21	slug-ft^2
	x_{cm}	56.4	in
	y_{cm}	0.00	in
	z_{cm}	11.5	in
Left wing sensors	x_p	+52.41	in
	y_p	−40.94	in
	z_p	+14.28	in
	x_a	+58.37	in
	y_a	−42.35	in
	z_a	+14.26	in
	x_f	+60.87	in
	y_f	−40.93	in
	z_f	+12.73	in
Nose sensors[2]	x_p	−16.26	in
	y_p	−0.02	in
	z_p	+9.50	in
	x_a	−10.30	in
	y_a	+1.40	in
	z_a	+9.40	in
	x_f	−7.80	in
	y_f	+0.03	in
	z_f	+7.75	in
Right wing sensors	x_p	+52.32	in
	y_p	+40.90	in
	z_p	+14.04	in
	x_a	+58.32	in
	y_a	+42.40	in
	z_a	+14.03	in
	x_f	+60.82	in
	y_f	+40.88	in
	z_f	+12.57	in

[1]Positions are given in the model frame, not the body frame
[2]Used for the GTM simulation only and not present on the T-2 aircraft

Figures

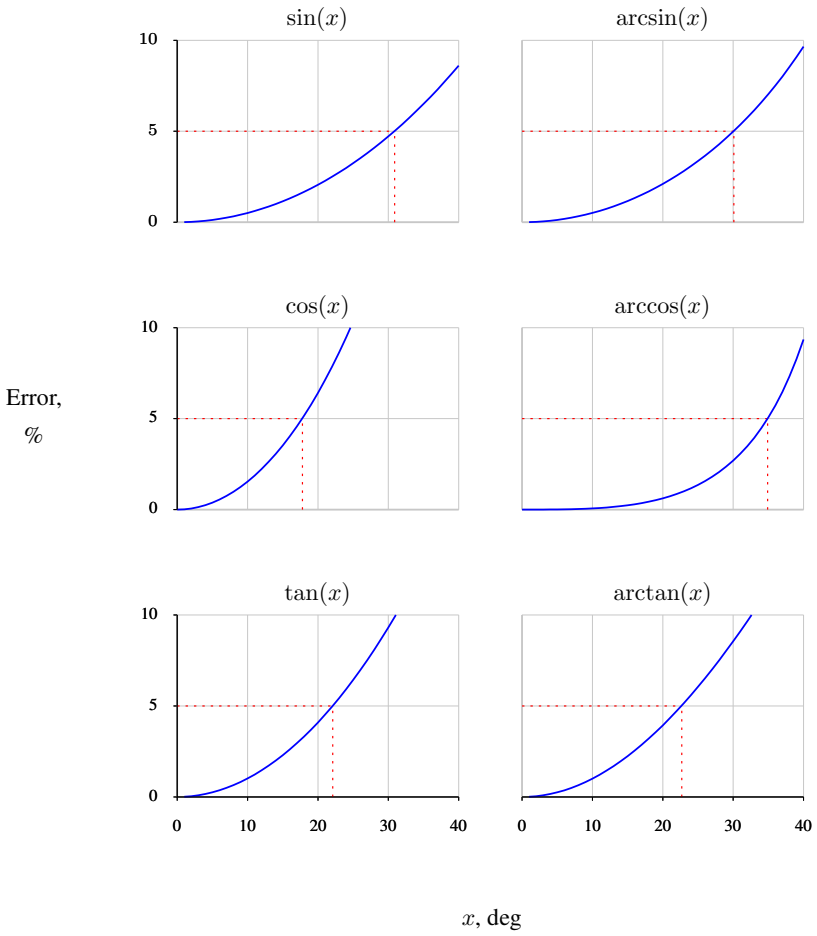

Figure 1: Relative error of small-angle approximations for several trigonometric functions, with 5% error highlighted

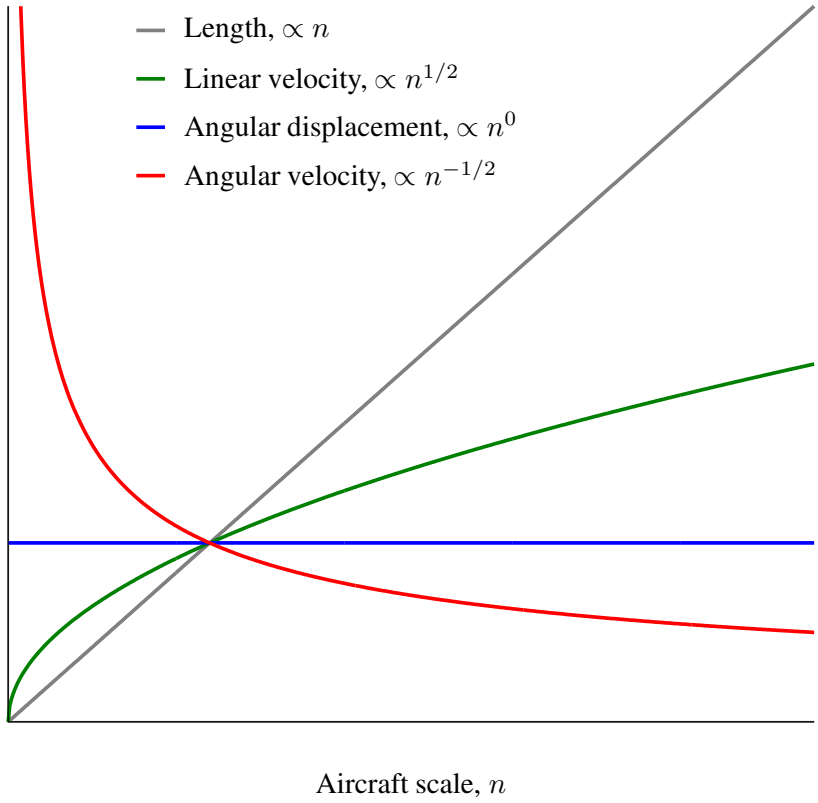

Figure 2: Variation of dynamic quantities with aircraft scale, from Ref. [7]

Figure 3: NASA T-2 airplane in flight (credit: NASA LaRC)

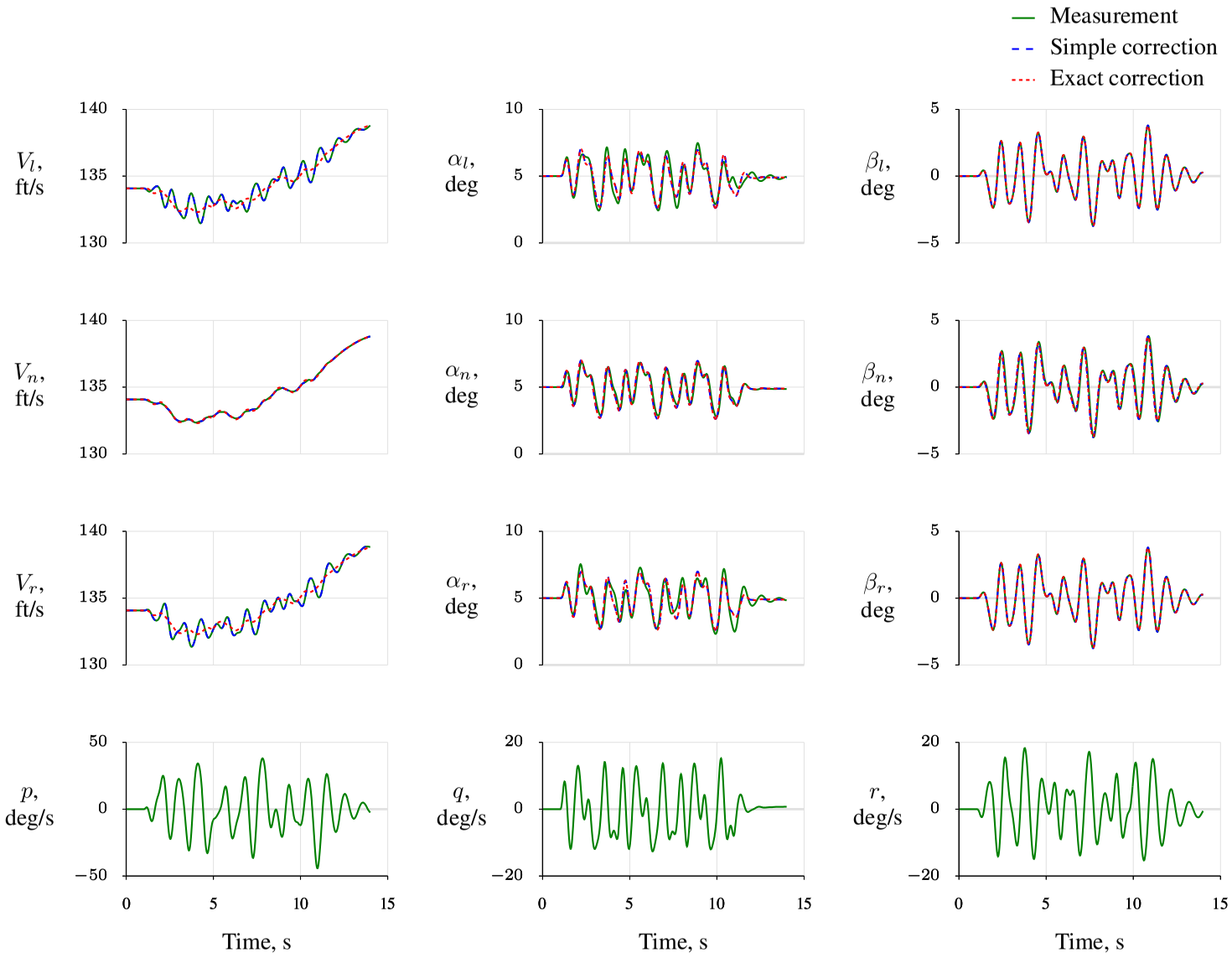

Figure 4: GTM simulation data: excitation from straight and level flight ($V_0 = 135$ ft/s, $\alpha_0 = 5.0$ deg, $h_0 = 4000$ ft)

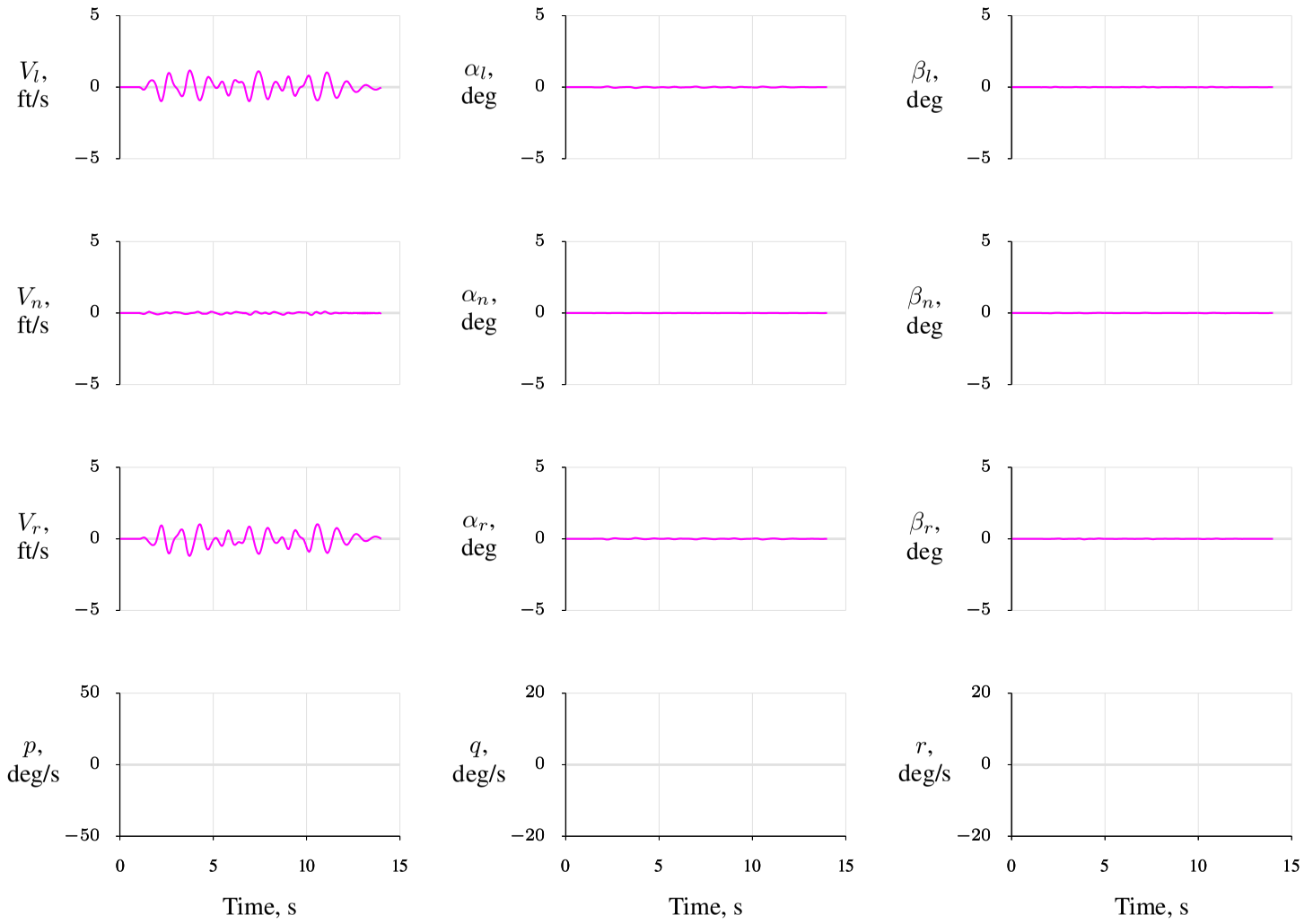

Figure 4: Differences between simple and exact corrections (Concluded)

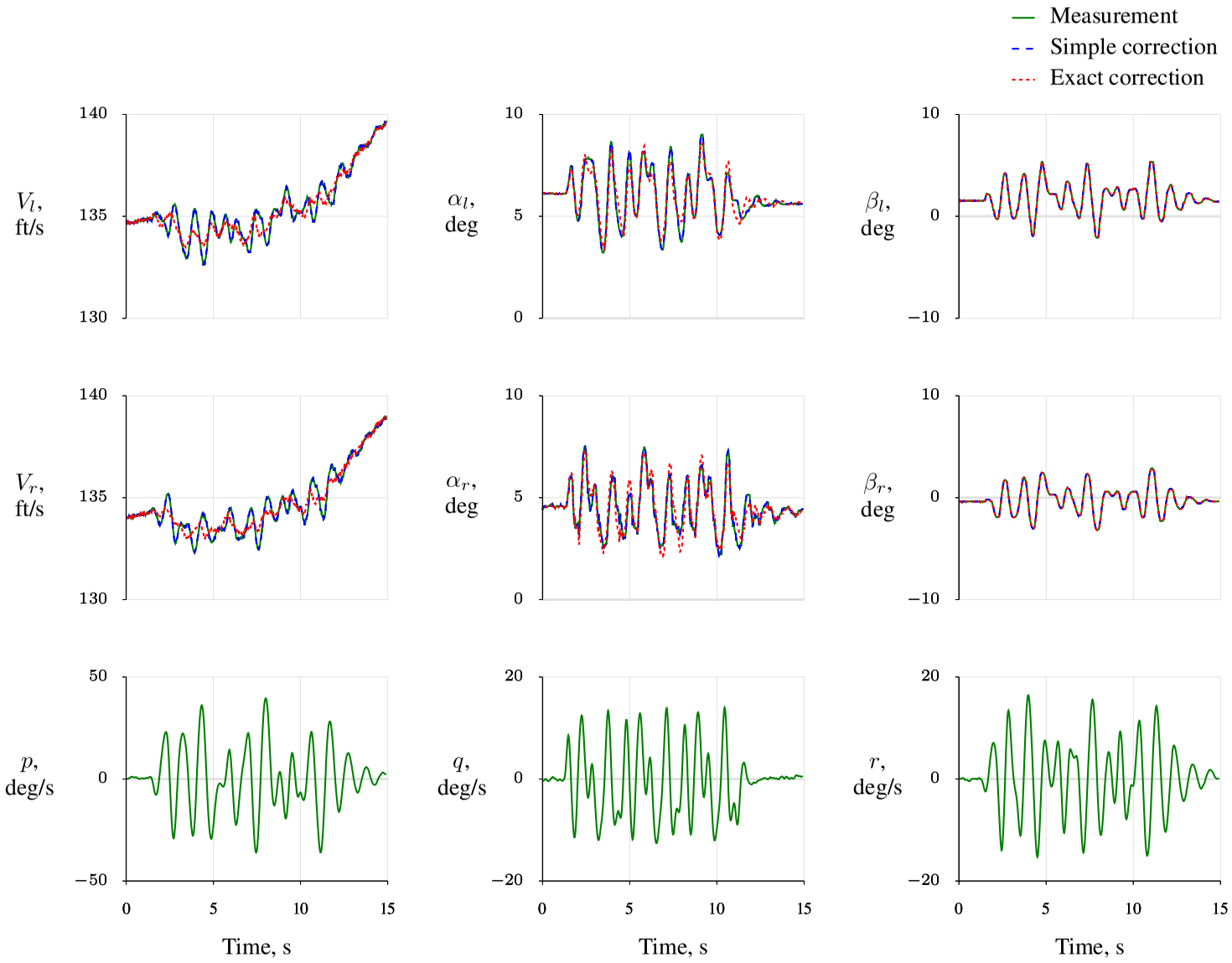

Figure 5: T-2 flight data: excitation from straight and level flight (Flight 33, Card 18, Maneuver B, $V_0 = 135$ ft/s, $\alpha_0 = 5.0$ deg, $h_0 = 1350$ ft)

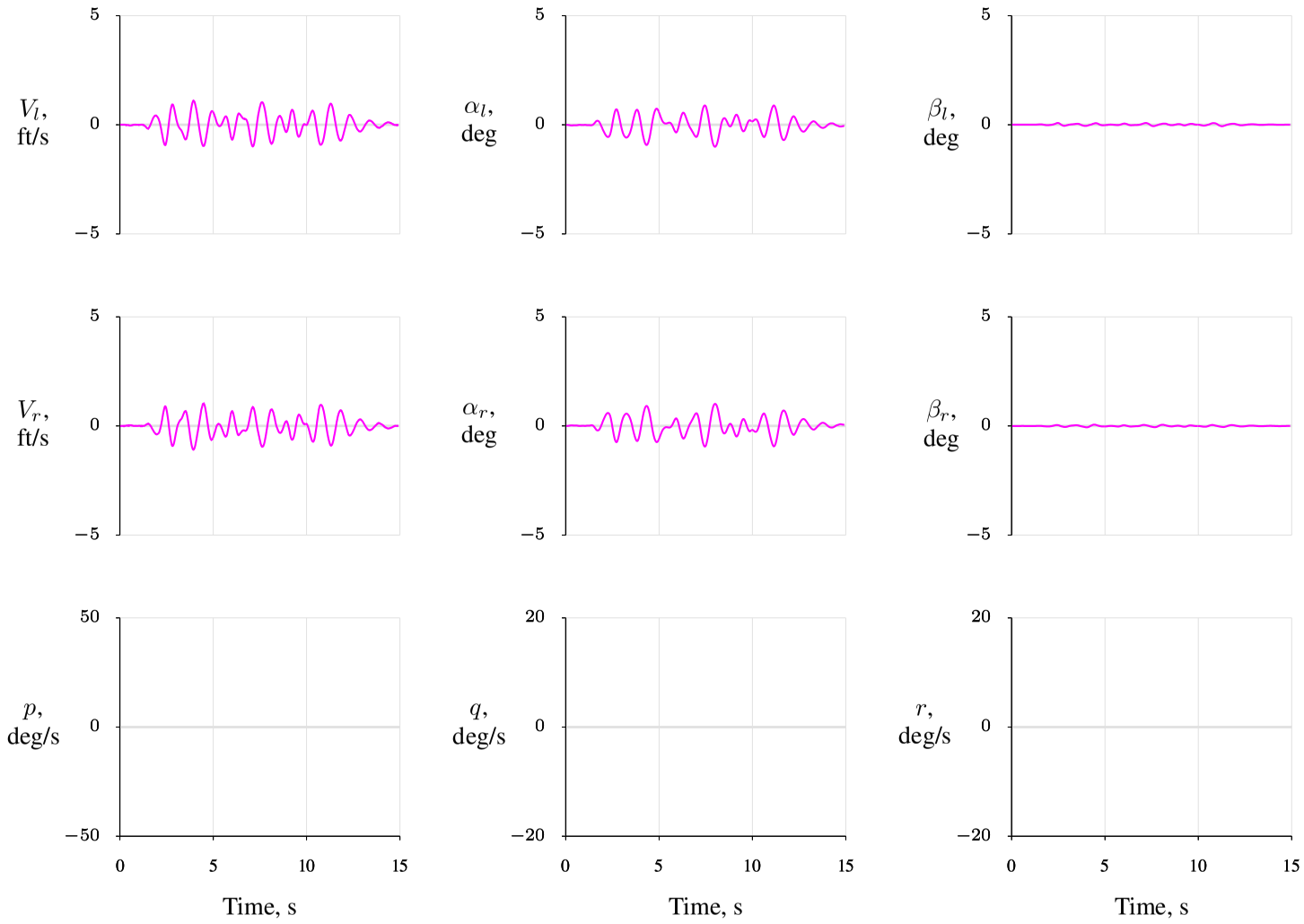

Figure 5: Differences between simple and exact corrections (Concluded)

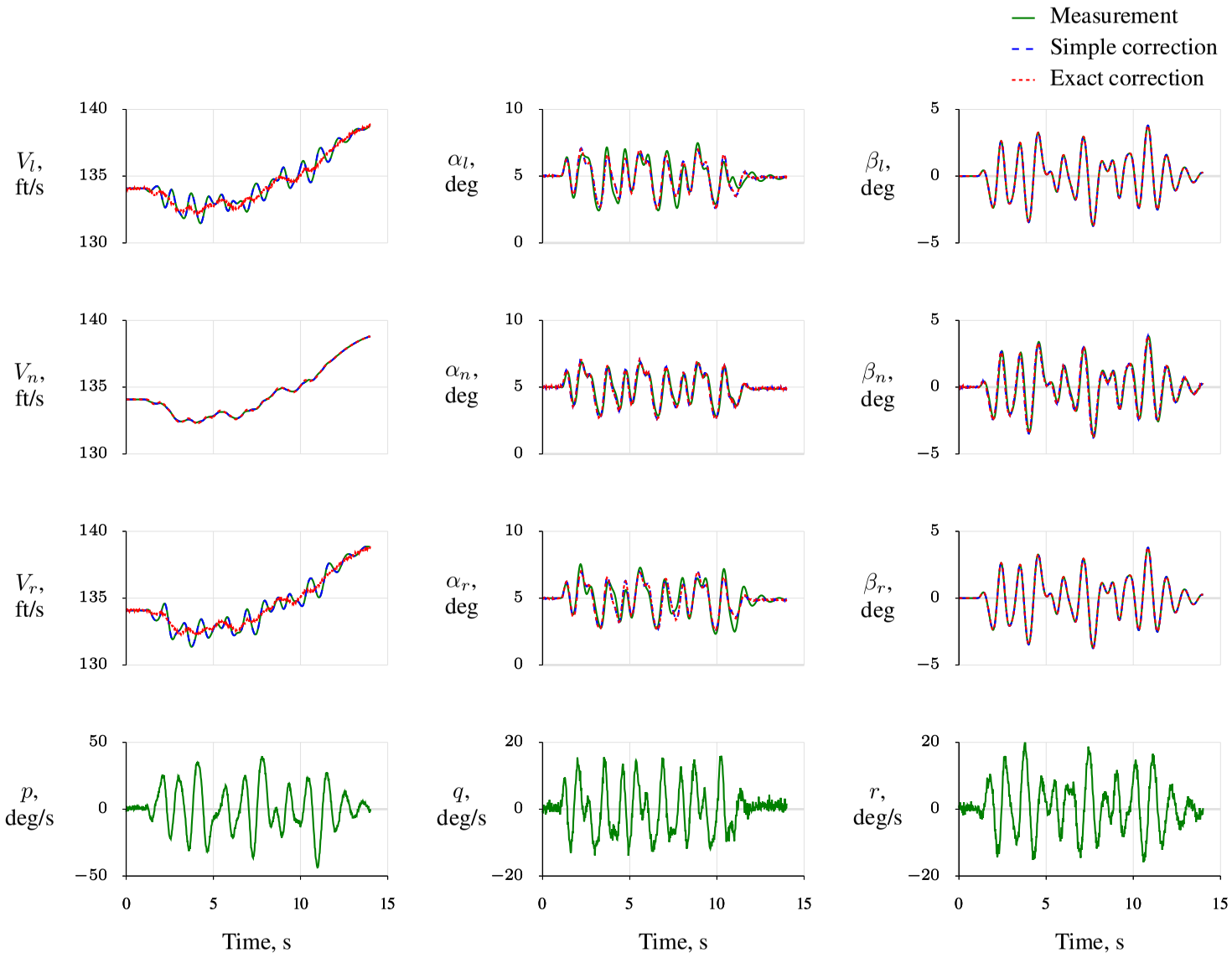

Figure 6: GTM simulation data: excitation from straight and level flight with measurement errors ($V_0 = 135$ ft/s, $\alpha_0 = 5.0$ deg, $h_0 = 4000$ ft)

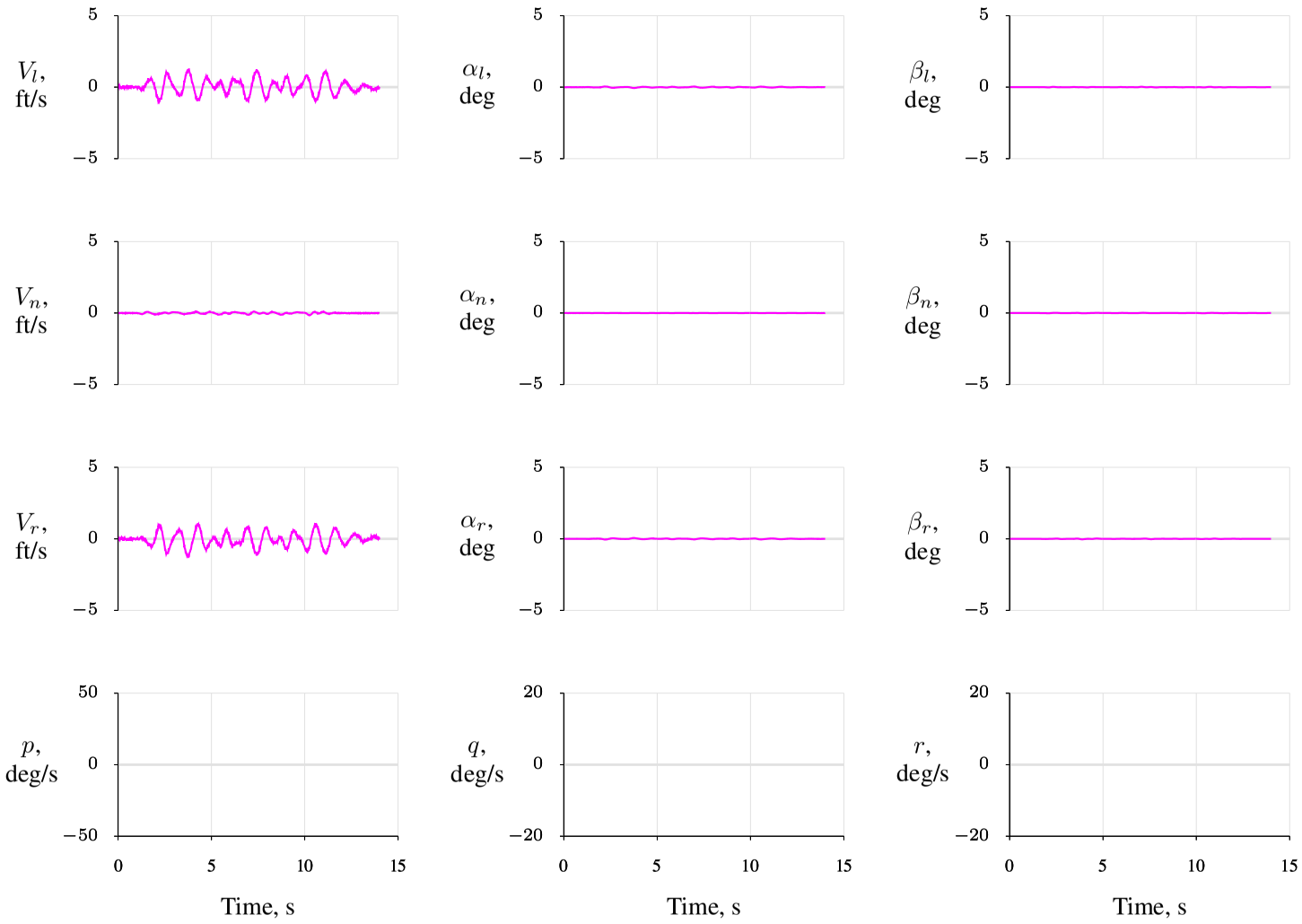

Figure 6: Differences between simple and exact corrections (Concluded)

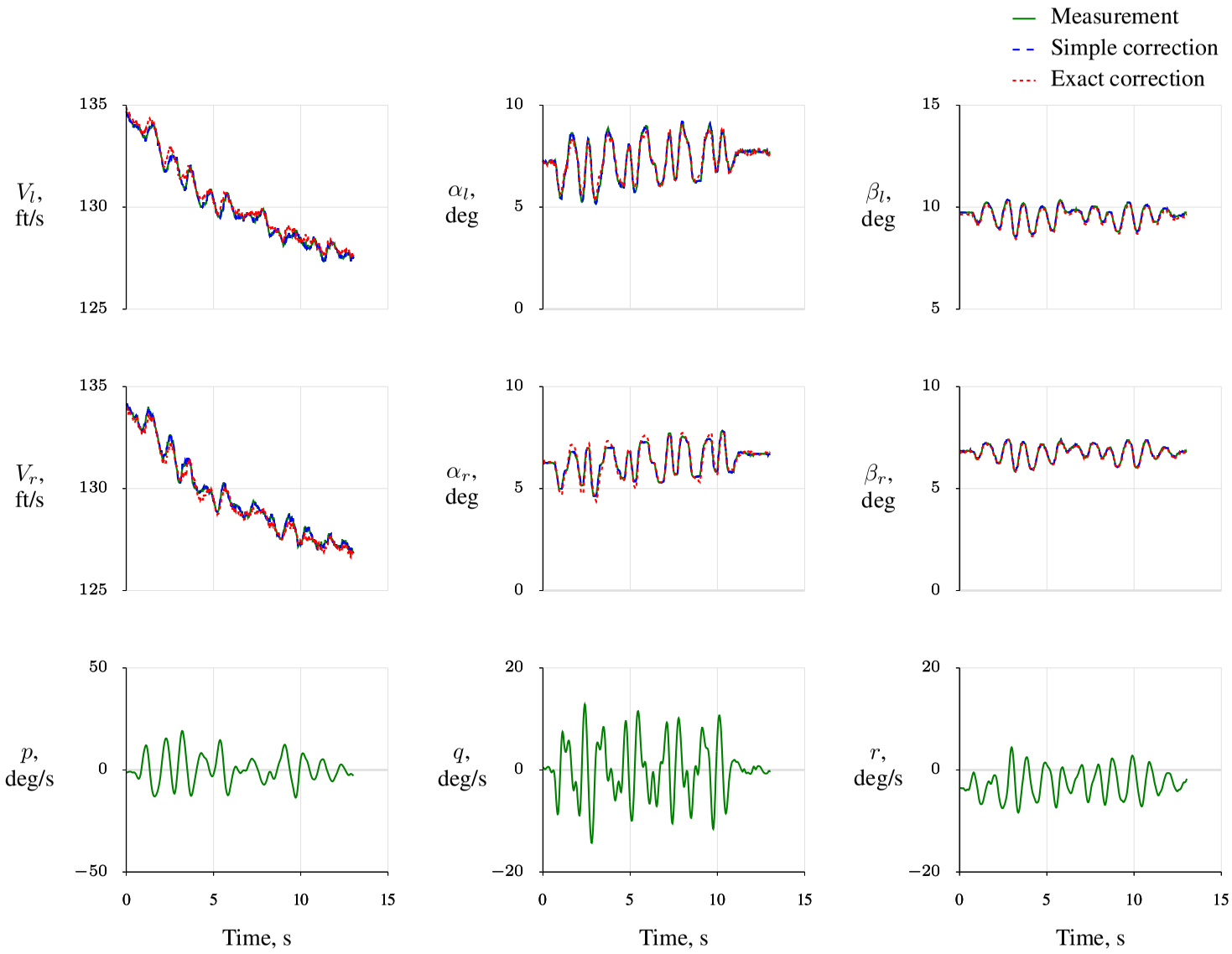

Figure 7: T-2 flight test data: excitation at high sideslip (Flight 12, Card 38, Maneuver A, $V_0 = 135$ ft/s, $\alpha_0 = 5.5$ deg, $\beta_0 = 7.8$, $h_0 = 1000$ ft)

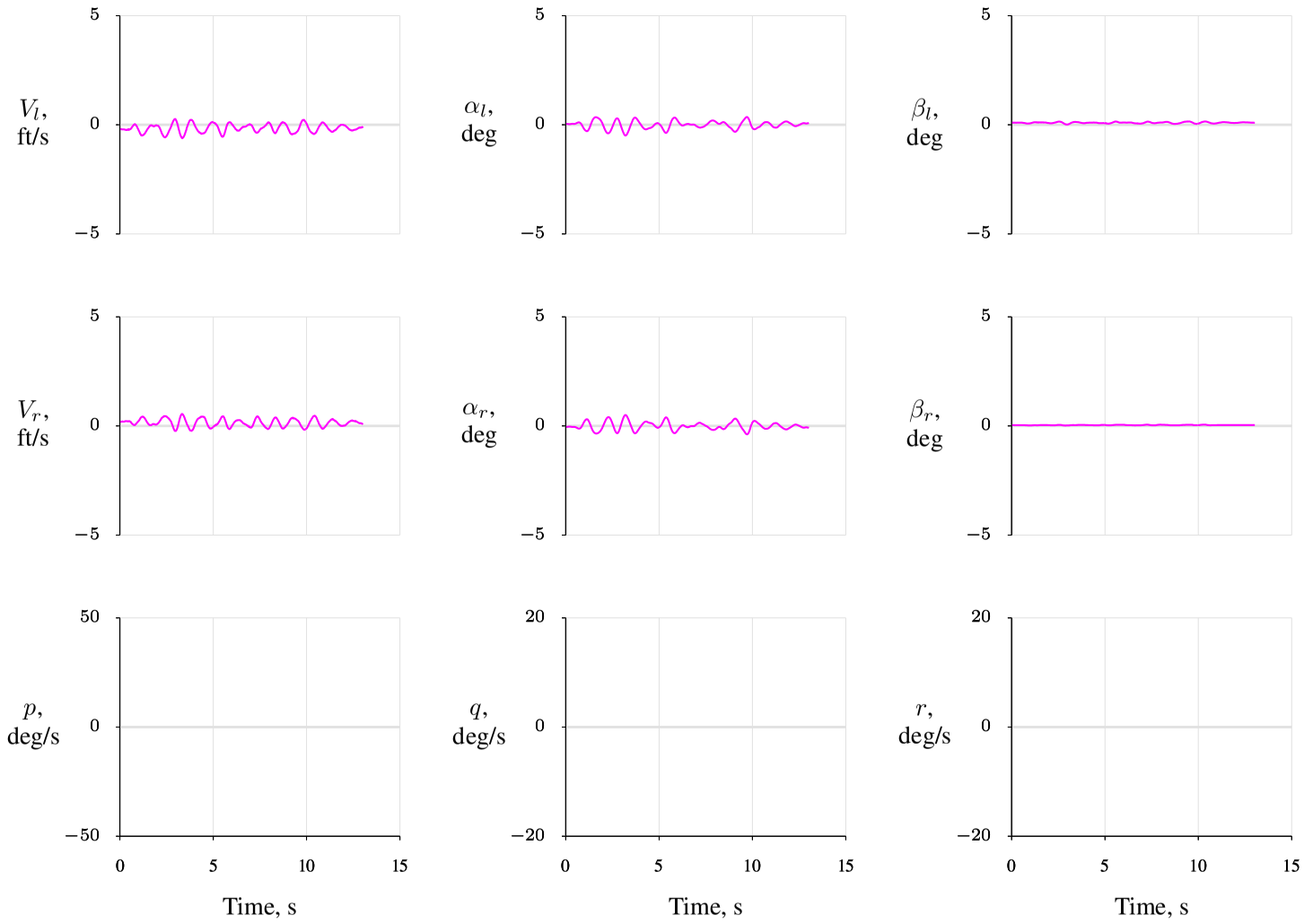

Figure 7: Differences between simple and exact corrections (Concluded)

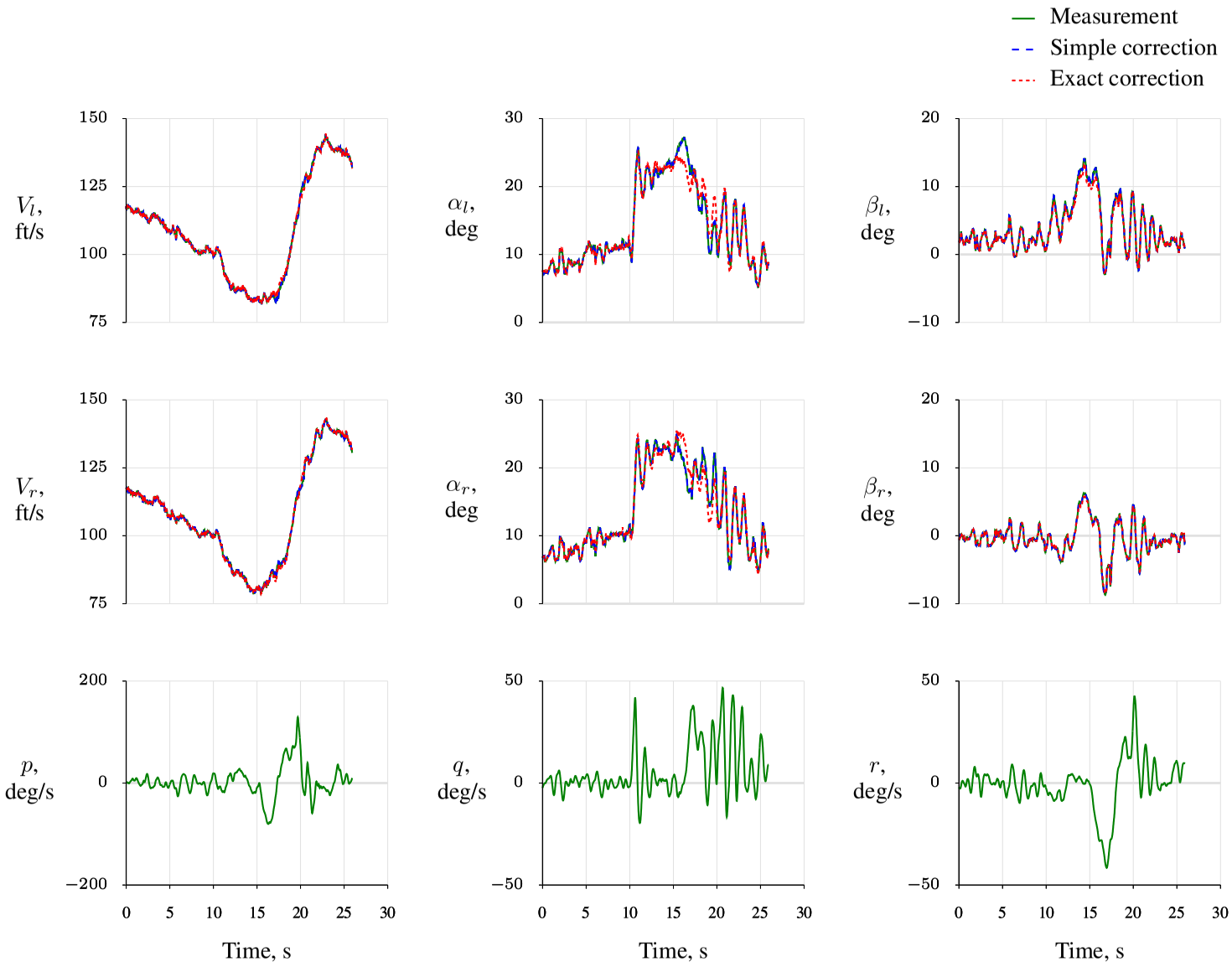

Figure 8: T-2 flight test data: excitation at high angle of attack (Flight 48, Card 13, Maneuver A, $V_0 = 120$ ft/s, $h_0 = 1550$ ft)

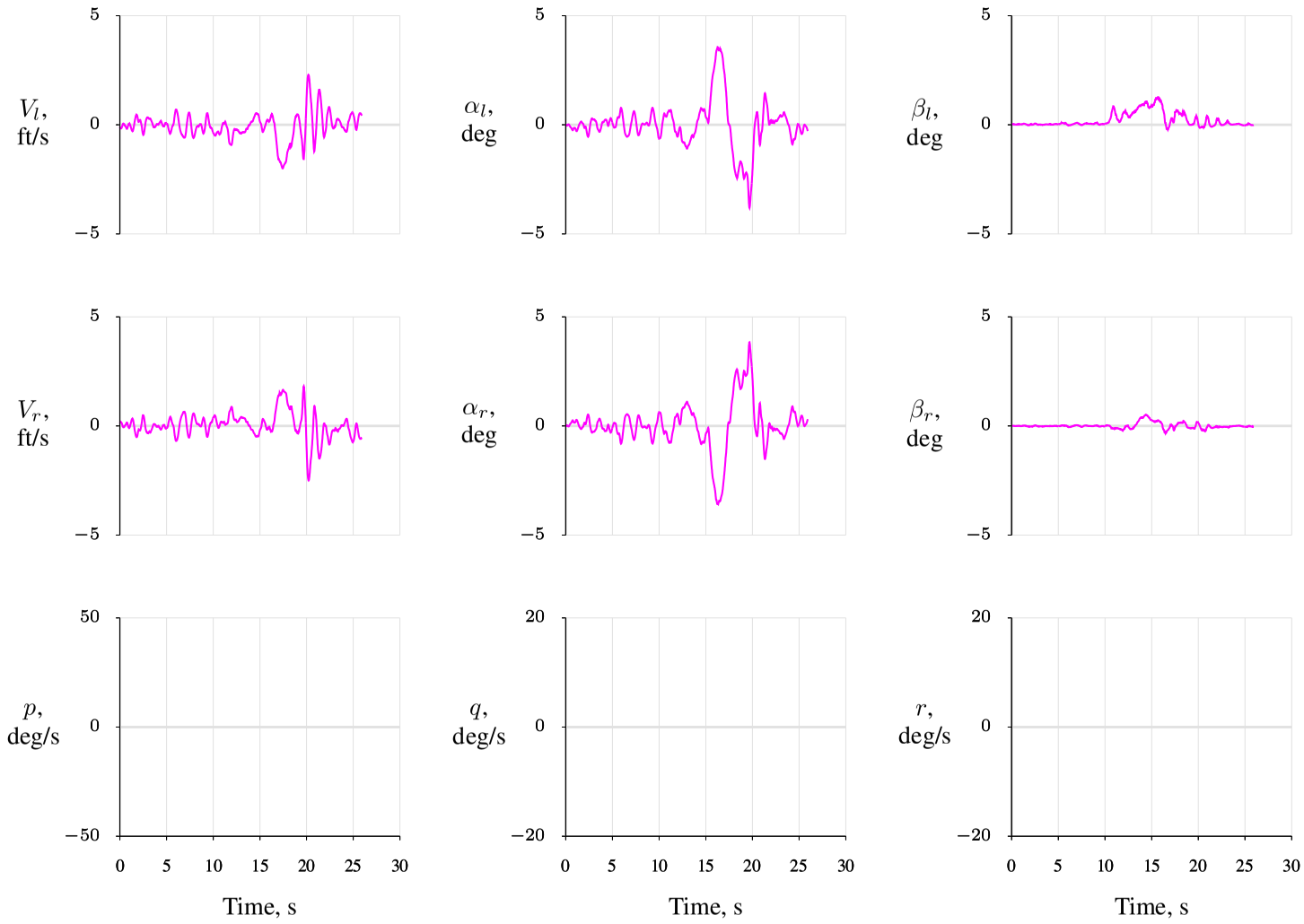

Figure 8: Differences between simple and exact corrections (Concluded)

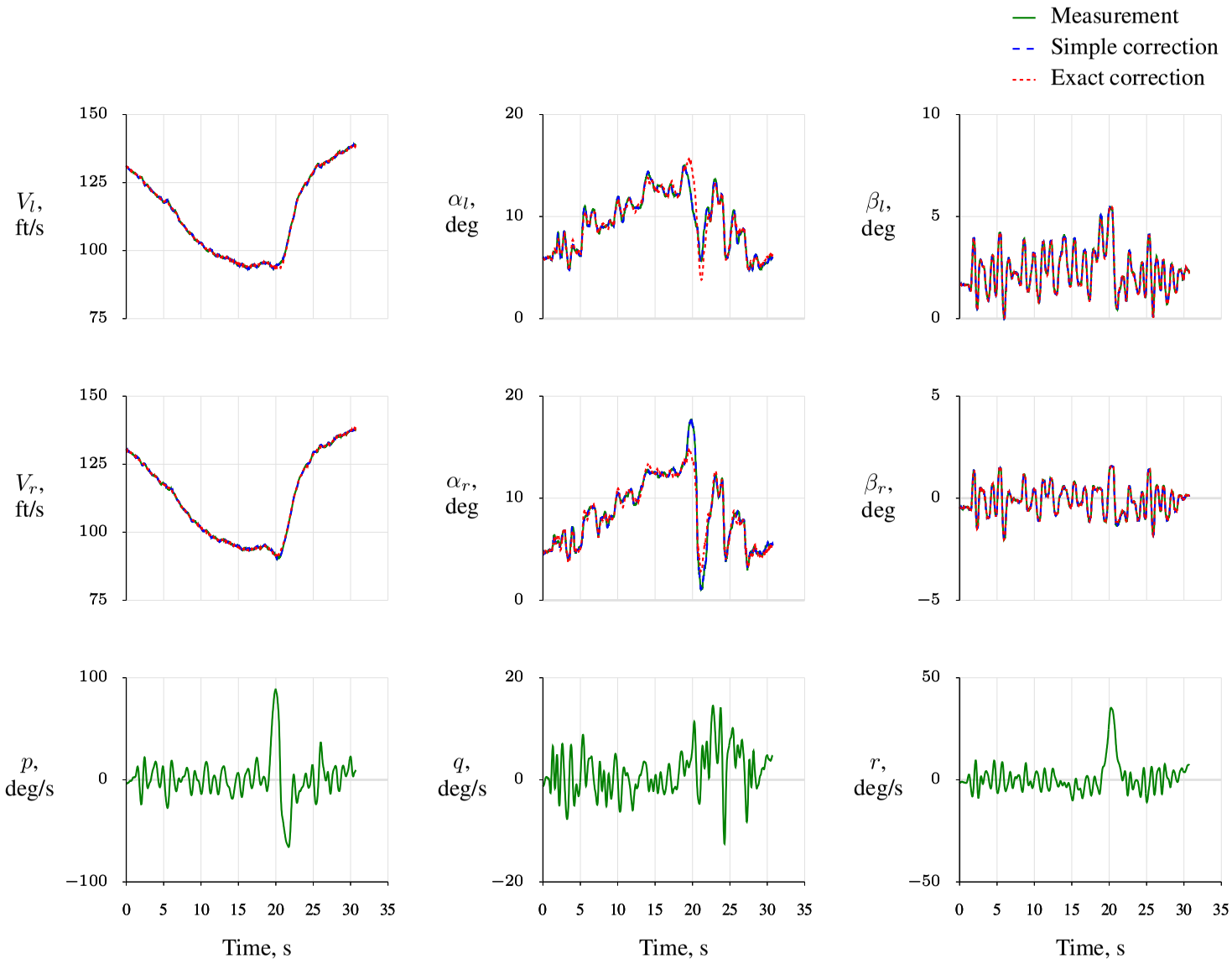

Figure 9: T-2 flight test data: excitation during a slow stall (Flight 42, Card 17, Maneuver B, $V_0 = 130$ ft/s, $h_0 = 1550$ ft)

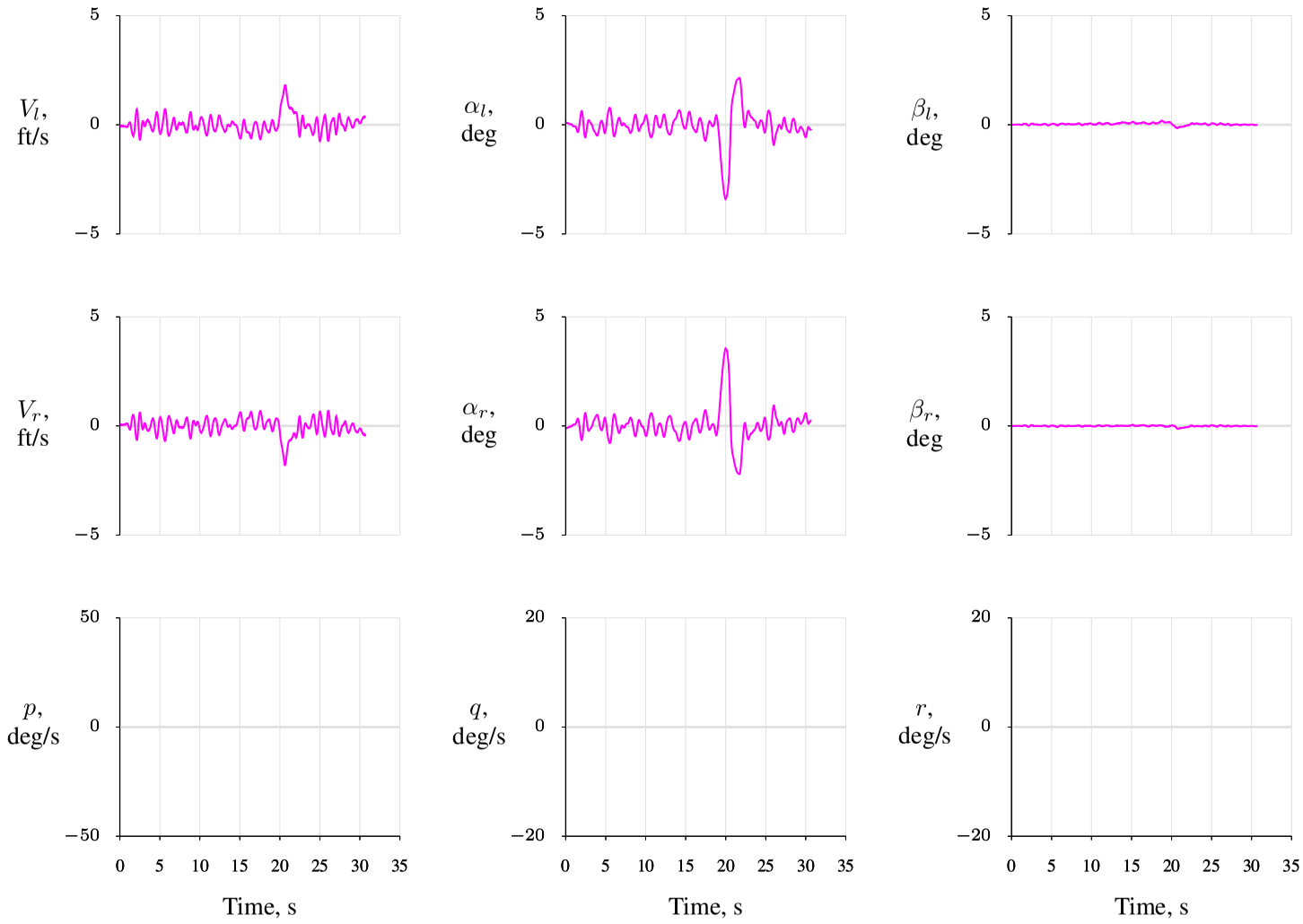

Figure 9: Differences between simple and exact corrections (Concluded)

REPORT DOCUMENTATION PAGE	Form Approved OMB No. 0704–0188

1. REPORT DATE *(DD-MM-YYYY)*	2. REPORT TYPE	3. DATES COVERED *(From - To)*
01-11-2017	Technical Memorandum	

4. TITLE AND SUBTITLE

Position Corrections for Airspeed and Flow Angle Measurements on Fixed-Wing Aircraft

5a. CONTRACT NUMBER

5b. GRANT NUMBER

5c. PROGRAM ELEMENT NUMBER

6. AUTHOR(S)

Jared A. Grauer
Langley Research Center, Hampton, Virginia

5d. PROJECT NUMBER

5e. TASK NUMBER

5f. WORK UNIT NUMBER
081876.02.07.02.01.01

7. PERFORMING ORGANIZATION NAME(S) AND ADDRESS(ES)

NASA Langley Research Center
Hampton, Virginia 23681-2199

8. PERFORMING ORGANIZATION REPORT NUMBER
L–20882

9. SPONSORING/MONITORING AGENCY NAME(S) AND ADDRESS(ES)

National Aeronautics and Space Administration
Washington, DC 20546-0001

10. SPONSOR/MONITOR'S ACRONYM(S)
NASA

11. SPONSOR/MONITOR'S REPORT NUMBER(S)
NASA/TM–2017–219795

12. DISTRIBUTION/AVAILABILITY STATEMENT

Unclassified-Unlimited
Subject Category 08
Availability: NASA STI Program (757) 864-9658

13. SUPPLEMENTARY NOTES

14. ABSTRACT

This report addresses position corrections made to airspeed and aerodynamic flow angle measurements on fixed-wing aircraft. These corrections remove the effects of angular rates, which contribute to the measurements when the sensors are installed away from the aircraft center of mass. Simplified corrections, which are routinely used in practice and assume small flow angles and angular rates, are reviewed. The exact, nonlinear corrections are then derived. The simplified corrections are sufficient in most situations; however, accuracy diminishes for smaller aircraft that incur higher angular rates, and for flight at high air flow angles. This is demonstrated using both flight test data and a nonlinear flight dynamics simulation of a subscale transport aircraft in a variety of low-speed, subsonic flight conditions.

15. SUBJECT TERMS

Airspeed, Flow angle, Position corrections, Flight data analysis

16. SECURITY CLASSIFICATION OF:			17. LIMITATION OF ABSTRACT	18. NUMBER OF PAGES	19a. NAME OF RESPONSIBLE PERSON
a. REPORT	b. ABSTRACT	c. THIS PAGE			STI Help Desk (email: help@sti.nasa.gov)
U	U	U	UU	36	19b. TELEPHONE NUMBER *(Include area code)* (757) 864-9658